Simulating Fluid-Phase Equilibria of Water from First Principles†

Matthew J. McGrath,‡,§ J. Ilja Siepmann,*,‡,§ I-Feng W. Kuo,§ Christopher J. Mundy,§ Joost VandeVondele,|| Jürg Hutter,⊥ Fawzi Mohamed,# and Matthias Krack#

Departments of Chemistry and of Chemical Engineering and Material Science and the Minnesota Supercomputing Institute, University of Minnesota, 207 Pleasant Street SE, Minneapolis, Minnesota 55455, Chemistry and Materials Science Directorate, Lawrence Livermore National Laboratory, Livermore, California 94550, Department of Chemistry, University of Cambridge, Lensfield Road, Cambridge CB2 1EW, United Kingdom, Physical Chemistry Institute, University of Zurich, Winterthurerstrasse 190, CH-8057 Zurich, Switzerland, and Laboratory of Physical Chemistry, ETH Zurich, USI-Campus, Via Giuseppe Buffi 13, CH-6904 Lugano, Switzerland

Received: June 30, 2005; In Final Form: August 12, 2005

Efficient Monte Carlo algorithms and a mixed-basis set electronic structure program were used to compute from first principles the vapor−liquid coexistence curve of water. A water representation based on the Becke−Lee−Yang−Parr exchange and correlation functionals yields a saturated liquid density of 900 kg/m^3 at 323 K and normal boiling and critical temperatures of 350 and 550 K, respectively. An analysis of the structural and electronic properties of the saturated liquid phase shows an increase of the asymmetry of the local hydrogen-bonded structure despite the persistence of a 4-fold coordination and decreases of the molecular dipole moment and of the spread of the lowest unoccupied molecular orbital with increasing temperature.

Introduction

Water holds a unique role among liquids, not only because of its ubiquity and importance on earth but also because of its anomalous liquid properties. Water's ability to act as donor and acceptor for two hydrogen bonds, which leads to the formation of a tetrahedral network, and its participation in many chemical processes, particularly self-dissociation and acid−base equilibria, have made understanding its properties a grand challenge for liquid state theory and molecular simulation.[1−3] The phase diagram holds a central role in thermodynamics, and only with its knowledge it is possible to make meaningful comparisons of experiment, theory, and simulation. For example, it would not be helpful to discuss whether a given water model can reproduce the well-known liquid-phase anomalies, such as the density maximum at $T = 277$ K and $p = 1$ atm or the (isothermal) compressibility minimum at $T = 320$ K and $p = 1$ atm, without first demonstrating that the liquid phase is actually thermodynamically stable at these conditions for the specific model.

Most particle-based molecular simulations of water use pairwise-additive, empirical interaction potentials and have provided a wealth of microscopic level information. In 1969, Barker and Watts[4] reported the first simulation of liquid water and discussed its structural properties. About 20 years later, the vapor−liquid coexistence curve of water was first computed,[5] and in 2004, the complete phase diagram was determined using two empirical water models.[6] However, empirical models struggle to describe water over a wide range of state points (from small water clusters in the atmosphere[7,8] to dense water in giant planets[9,10]) that involve dramatic changes of its electronic structure.

In contrast, an ab initio representation of water affords the opportunity to study both physical and chemical properties. The first Car−Parrinello molecular dynamics (CPMD) simulation[11] for liquid water employing a quantum-mechanical description of the molecular interactions was performed in the early 1990s.[12] Although ab initio molecular dynamics simulations have contributed to a better understanding of structural, dynamical, and electronic aspects of neat liquid water,[13−21] supercritical fluid water,[22−24] aqueous solutions,[25,26] and the air−water interface,[27] little research has been done to evaluate the thermodynamic properties (e.g., chemical potential, enthalpy of vaporization, or normal boiling point) of first principles descriptions of water, and in fact, until this work it has not been known whether common density functional descriptions of water yield a stable liquid phase at ambient conditions. The notable exception is recent work by Asthagiri et al.,[28] who used a combination of ab initio molecular dynamics and quasichemical theory to estimate the free energy of hydration of liquid water at near-ambient conditions and reported values of −21 and −60 kJ/mol for two different density functionals. This large spread demonstrates the computational challenges for accurate predictions of the free energy of fluid phases at low pressure from first principles, whereas significant advances have been made for solid−solid and solid−liquid equilibria at high pressures.[29,30]

Simulation Methodology

For the present research, we use Gibbs ensemble Monte Carlo (MC) simulations[31] to directly calculate the vapor−liquid coexistence properties of water. The first principles MC simulations of this work were performed using the computer program CP2K (http://cp2k.berlios.de/), which expands the Kohn−Sham orbitals

† Part of the special issue "Donald G. Truhlar Festschrift".

* To whom correspondence should be addressed. E-mail: siepmann@chem.umn.edu.

‡ University of Minnesota.

§ Lawrence Livermore National Laboratory.

|| University of Cambridge.

⊥ University of Zurich.

ETH Zurich.

10.1021/jp0535947 CCC: $33.50
Published on Web 09/21/2005

using a linear combination of atom-centered Gaussian-type orbital functions and describes the electronic charge density with an auxiliary basis set of plane waves.[32,33] The Gibbs ensemble MC simulations utilize two separate simulation boxes for the vapor and liquid phases (i.e., the phases are in thermodynamic contact but do not share an explicit interface) and employ five different types of moves: (i) translations of rigid molecules, (ii) rigid-body rotations around the molecular center of mass, (iii) conformational moves altering either bond length or angle, (iv) volume exchanges between the two boxes, and (v) particle swaps between the two boxes. The first three types serve to establish thermal equilibrium, the fourth yields mechanical equilibrium, and the fifth equalizes the chemical potential of water between the phases. Details of the CP2K program for first principles MC simulations of water in the canonical ensemble using move types i to iii have been reported elsewhere.[19] Standard volume moves with scaling of only the molecular center-of-mass coordinates are employed.[34,35] To improve the efficiency of the particle swap moves, a multistep configurational-bias MC approach is used.[36−38] First, the potential energies of 640 trial insertions and its Rosenbluth weight are evaluated using an inexpensive potential.[39] Thereafter, one suitable trial position is selected from this pool using the Boltzmann weights calculated for the inexpensive potential, and its ab initio energy is evaluated. The final acceptance step for this swap move then corrects for the energy difference between the inexpensive and ab initio energies.[37,38,40]

Although there is general agreement that low-frequency *inter*-molecular "vibrations" (including the librational mode and the three-molecule antisymmetric stretching of a hydrogen-bonded trimer as identified by Silvestrelli et al.[41]) are well reproduced using classical mechanics (i.e., using molecular translations and rotations), it is important to comment on our choice to classically sample conformational changes using move type iii. The characteristic vibrational temperatures for water's three vibrational modes (5360, 5160, and 2290 K in the gas phase) are well above its supercritical temperature. Although there is not enough thermal energy to excite these quantal vibrational modes, it needs to be recognized that the intermolecular interactions in the liquid phase are sufficiently strong to alter water's conformation,[13,42] thereby leading to large shifts and substantial broadening in the vibrational spectrum associated with the transfer from the vapor phase to the liquid phase.[41,42] Furthermore, the classical vibrational amplitudes are substantially smaller than the quantum-mechanical zero-point amplitudes. Thus, classically sampling conformational rearrangements caused by changes in the local environment appears to be more preferable than keeping the internal conformation of the nuclei rigid, while allowing the electronic structure to change. The enhanced classical heat capacity arising from the (harmonic) *intra*-molecular vibrational modes will not alter the phase diagram because both phases are affected to the same extent, and the vibrational heat will cancel in the computation of the heat of vaporization.[43]

The Gibbs ensemble MC simulations were performed at T = 323, 373, 423, 473, and 523 K for a system consisting of a total of 64 water molecules. Albeit a rather small system size, an exploratory Gibbs ensemble investigation using the empirical TIP4P model[44] (together with the usual tail correction and Ewald summations) demonstrates converged saturation properties near the boiling point (see Figure 1).

The initial configurations were prepared using the final configuration of a canonical ensemble MC simulation[19] at T = 315 K and $\rho = 10^3$ kg/m^3 that was scaled to the experimental saturated liquid density at the temperature of interest. For one temperature (T = 473 K), a second independent run was started by scaling the configuration of another canonical ensemble MC simulation[19] to a lower density. The volume of the initially empty vapor box was set equal to the initial liquid volume. For the higher temperatures, short CPMD trajectories of 1−2 ps were used to preequilibrate the configurations because molecular dynamics is more efficient in relaxing the collective modes following the dramatic change in density (upon scaling from $\rho = 10^3$ kg/m^3 to the experimental saturated liquid density).

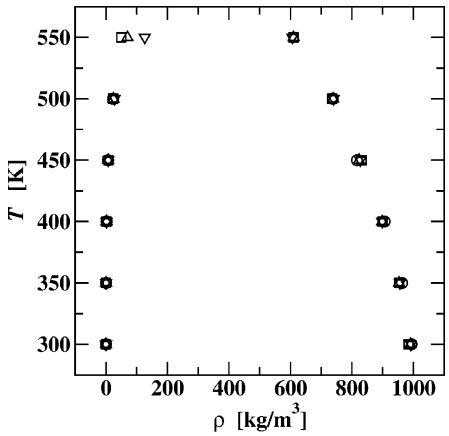

Figure 1. Vapor−liquid coexistence curve for the TIP4P model. Results from Gibbs ensemble simulations using 32, 64, 128, and 256 are depicted by ○, □, △, and ▽, respectively. The corresponding normal boiling points are 364 ± 2, 364 ± 2, 365 ± 2, and 364 ± 1 K, respectively.

The lengths of the simulations are measured in MC cycles, where it should be noted that one cycle corresponds to 64 ab initio energy calculations (i.e., the number of presampling moves for translations, rotations, and conformational changes using the approximate potential is significantly larger).[19] The simulations were run for 350−450 MC cycles, and the ensemble averages were calculated from the last 200 cycles. As for the system size, the large computational expense of these first principles calculations necessitates much shorter simulation lengths than typical for simple pairwise additive potentials. Again, we have turned to simulations for the TIP4P model to obtain an estimate of the precision of very short simulations. To this extent, we followed a procedure mimicking the CP2K runs. First, five independent configurations were generated for TIP4P water at T = 300 K and $\rho = 10^3$ kg/m^3. These five configurations were then scaled to either the experimental or BLYP (obtained in the present work) coexistence densities at T = 373 and 473 K. For each temperature and initial liquid density, five independent simulations were carried out for the TIP4P model that used equivalent numbers of translation, rotation, volume exchange, and particle swap moves (but no conformational moves for the rigid TIP4P model) as used for the first principles simulations. These simulations yielded the following data with the standard deviation computed from the five independent runs: (a) 373 K and started from the experimental coexistence density: ρ_{liq} = 932 ± 17 kg/m^3 and ρ_{vap} = 1.09 ± 0.27 kg/m^3; (b) 373 K and started from the BLYP coexistence density: ρ_{liq} = 926 ± 14 kg/m^3 and ρ_{vap} = 0.94 ± 0.14 kg/m^3; (c) 473 K and from experiment: ρ_{liq} = 794 ± 54 kg/m^3 and ρ_{vap} = 15.6 ± 6.4 kg/m^3; (d) 473 K and from BLYP: ρ_{liq} = 773 ± 45 kg/m^3 and ρ_{vap} = 11.9 ± 2.9 kg/m^3. As can be seen, the simulations started from different initial densities agree to within one standard deviation. Furthermore, the corresponding results for long simulations (50,000 cycles divided into 5 blocks) are ρ_{liq} = 935 ± 14 kg/m^3 and ρ_{vap} = 0.84 ± 0.18 kg/m^3 (at 373 K) and ρ_{liq}

$= 796 \pm 3$ kg/m^3 and $\rho_{vap} = 16.9 \pm 2.6$ kg/m^3 (at 473 K). These results nicely demonstrate the convergence and statistical uncertainties that should be expected for the relatively short first principles simulations.

The electronic structure parameters used in the Gibbs ensemble MC simulations were as follows: the Becke−Lee−Yang−Parr (BLYP) exchange and correlation energy functionals[45,46] together with a triple-ζ valence basis set with two sets of *d*-type or *p*-type polarization functions (TZV2P), the norm-conserving pseudo-potentials of Goedecker and co-workers (GTH),[47,48] and a relatively large charge density cutoff at 1200 Ry for the auxiliary plane wave basis set. Here it should be noted that after extensive tests of different basis sets, Handy and co-workers[49] recommended TZV2P as the most appropriate basis set for generalized gradient approximation (GGA) functionals. This is also supported by a recent evaluation using the CP2K program.[33] These assessments of basis set effects have concentrated on gas-phase structures, and an equivalent recommendation for condensed phases is still lacking. There is certainly the possibility that inclusion of diffuse functions may impact the cohesive energy and, hence, the vapor−liquid equilibria. In passing, it should be noted that simulations in the microcanonical and canonical ensembles showed very good agreement for the structural properties of water using either a plane wave or mixed basis set approach.[19] The large charge density cutoff is necessitated by the fluctuating volume[35] present in Gibbs ensemble simulations.

With these parameters a Gibbs ensemble MC cycle requires approximately 4 h on 48 nodes of Thunder (http://www.llnl.gov/linux/thunder/). The significantly greater expense of these Gibbs ensemble simulations over previous simulations in the canonical ensemble[19] arises from the use of two simulation boxes (and, in contrast to pairwise additive potentials, the computation of the ab initio energy for a vapor box containing only a single molecule is rather expensive), the larger charge density cutoff (1200 vs 280 Ry), and the fact that particle swap and volume exchange moves yield a sequence of configurations characterized by rather dramatic changes. Therefore, schemes that generate a satisfactory initial electronic wave function based on the assumption of continuity cannot be employed here, and the computational cost of the full SCF energy evaluation is significantly increased as compared to conventional simulations in the canonical ensemble.

In the closing of this section, we would like to address the neglect of nuclear quantum effects in this study. Recently, two independent studies[50,51] have pointed out that a discretization of $\mathcal{O}(10^2)$ is required to yield converged path integral simulations for water. Unfortunately, the already large expense of the present Gibbs ensemble simulations does not allow for the additional expense arising from a converged path integral treatment. However, from a comparison of the vapor−liquid coexistence curves and other thermodynamic properties for H_2O, D_2O, and T_2O (e.g., the normal boiling points of the latter are 374.6 and 374.7 K, respectively), one might argue that the statistical uncertainties of the present simulations are larger than the systematic error arising from the neglect of the nuclear quantum effects. In passing, we might notice that the effect of nuclear quantization on the specific density of *n*-alkanes has been investigated, and a density decrease of about 2% from classical to path integral simulations was observed.[52]

Results and Discussion

Phase Diagram. Figure 2 shows the instantaneous values of the vapor and liquid densities and the heat of vaporization, respectively, observed throughout the MC trajectories for the two independent simulations at $T = 473$ K. It appears that both systems have reached equilibrium after about 150 MC cycles (as evidenced by the decrease from the higher initial densities and the settling of the vapor densities following an initial increase) and that the cumulative averages of the two independent simulations computed over the last 200 cycles agree to within a few percent. These observations are consistent with the exploratory simulations for the TIP4P model described above.

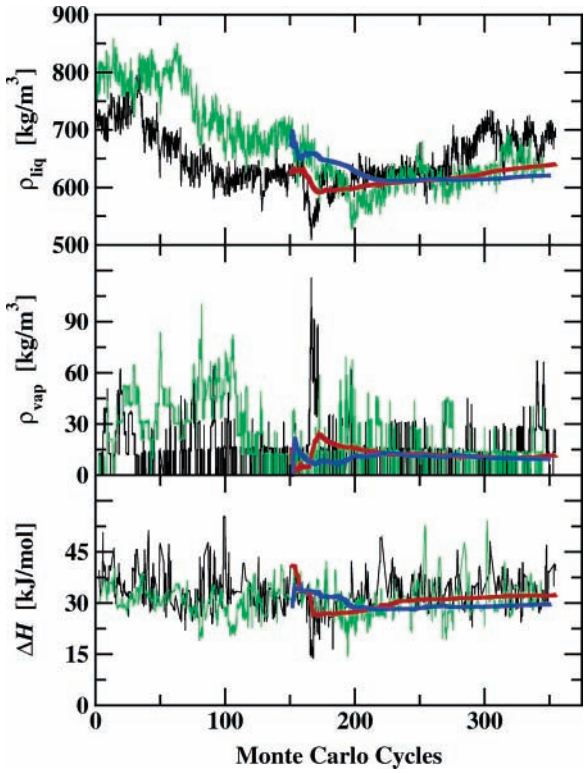

Figure 2. Instantaneous values and cumulative averages (only for the last 200 MC cycles) of the saturated liquid and vapor densities and of the heat of vaporization versus the number of MC cycles. The black/red and green/blue lines depict two independent MC simulations at $T = 473$ K that were started from configurations with different initial densities.

The fluctuations in the heat of vaporization are relatively large as compared to simulations for rigid water molecules using an empirical potential, but it should be recognized that these MC simulations also involve sampling of the vibrational degrees of freedom. A given presampling sequence can involve molecules in both phases. That is, a decrease in the potential energy of the vapor phase might be compensated by an increase in the energy of the liquid phase and vice versa to lead to the acceptance of the move sequence, but these changes can add together for a larger change in the heat of vaporization.

The vapor−liquid coexistence curve, the Clausius−Clapeyron plot of the saturated vapor pressure,[53] and the temperature dependence of the heat of vaporization are shown in Figures 3−5. The BLYP-GTH-TZV2P-1200 representation yields two-phase coexistence over the temperature range from 323 to 523 K, a very encouraging result. Although the coexistence properties of water are qualitatively reproduced, there are noticeable deviations from experiment.[54] The saturated liquid densities of the BLYP-GTH-TZV2P-1200 representation fall below and the saturated vapor pressures (with the exception of $T = 423$ K) lie above their experimental counterparts over the entire two-phase envelope. A fit of the computed coexistence curve using

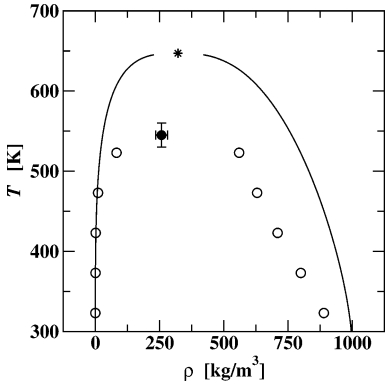

Figure 3. Vapor−liquid coexistence curve. The line and asterisk depict the experimental data,[54] and the simulation results and the estimated critical point for the BLYP-GTH-TZV2P-1200 description of water are shown as open and filled circles, respectively.

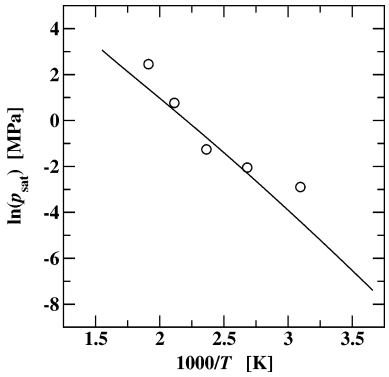

Figure 4. Clausius−Clapeyron plot of the logarithm of the saturated vapor pressure[53] vs the inverse temperature. The line and circles depict the experimental data[54] and the simulation results for the BLYP-GTH-TZV2P-1200 description of water, respectively.

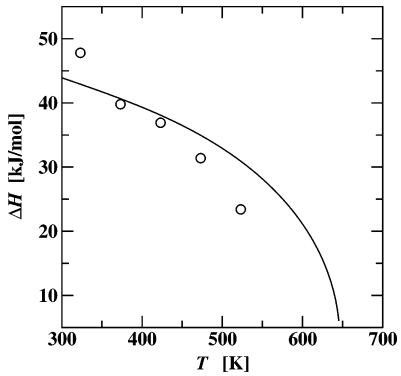

Figure 5. Temperature dependence of the heat of vaporization. The line and circles depict the experimental data[54] and the simulation results for the BLYP-GTH-TZV2P-1200 description of water, respectively.

the scaling law yields a critical temperature of 550 K (i.e., 15% below the experimental value), and a fit to the Clausius−Clapeyron equation points to a boiling point of about 350 K for the BLYP-GTH-TZV2P-1200 model. The heat of vaporization is well reproduced at intermediate temperatures.

There are many reasons that may be responsible for the quantitative discrepancies in the vapor−liquid coexistence properties between the BLYP-GTH-TZV2P-1200 representation and experiment. Among them are certainly that GGA functionals (as also other exchange and correlation functionals) do not satisfactorily describe dispersive interactions, that different density functional models yield different descriptions of the liquid phase,[55] and that BLYP and other GGA functionals do not quantitatively reproduce the binding energies of small water

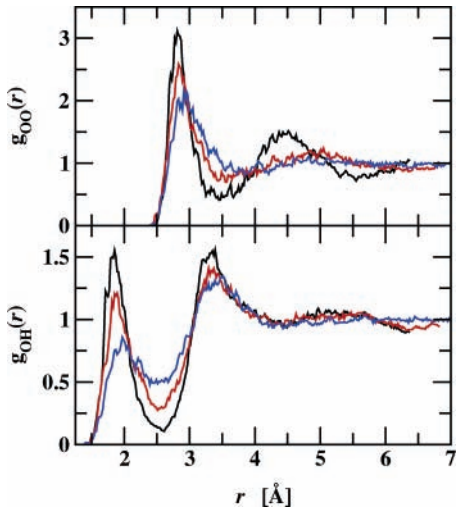

Figure 6. Temperature dependence of the oxygen−oxygen (top) and oxygen−hydrogen (bottom) radial distribution functions observed for the saturated liquid phase of BLYP-GTH-TZV2P-1200 water. The results at $T = 323$, 423, and 523 K are shown as black, red, and blue lines, respectively.

clusers.[56] Although a TZV2P basis set has been recommended for density functional calculations[49] and a charge density cutoff of 1200 Ry yields converged energies for this system, it is possible that use of a smaller basis set or cutoff might lead to better agreement with experiment due to cancellation of errors. For example, first principles MC simulations in the isobaric−isothermal ensemble have shown that a decrease in the cutoff to 280 Ry yields a higher (i.e., closer to experiment) specific density at ambient conditions than obtained for the cutoff of 1200 Ry used here.[35]

Structural Properties. Selected radial distribution functions (RDFs) for the saturated liquid phase are shown in Figure 6. The oxygen−oxygen and oxygen−hydrogen RDFs at 323 K agree well with those observed in canonical ensemble simulations[19] at 315 K and $\rho = 1000$ kg/m^3. The liquid phase is seen to significantly disorder with increasing temperature, and only the first solvation shell is discernible at 523 K, but the coordination numbers (computed from the value of the corresponding number integral at the first minimum of the RDF) yield a value of 4 over the entire temperature range, whereas substantially larger coordination numbers have been found for supercritical fluid water.[24] The first peak in the intermolecular oxygen−hydrogen RDF at about 1.8 Å signals that linear hydrogen bonding is present in the saturated liquid phase at all temperatures.

Recently, two experimental studies[57,58] have examined the structure and energetics of this first solvation shell and reached somewhat different conclusions. To probe the local asymmetry, the four nearest oxygen atoms around a given water molecule were identified, and the temperature dependence of the distribution of oxygen−oxygen distances and of the mean values for the two closest and the other two neighbors were computed (see Figures 7 and 8). As can be seen from the distributions, there is an asymmetry of the local coordination even at 323 K that becomes more pronounced as the temperature increases. However, this asymmetry appears more askew at larger distances with increasing temperature than as a shoulder at a given distance that increases in intensity. The distance to the two nearest oxygens in the 4-fold coordination shell increases only by 0.2 Å over the 200 K range, whereas the distance to the other two oxygens increases by 0.5 Å (i.e., a local structure with two strong and two distorted hydrogen bonds emerges).[57,58]

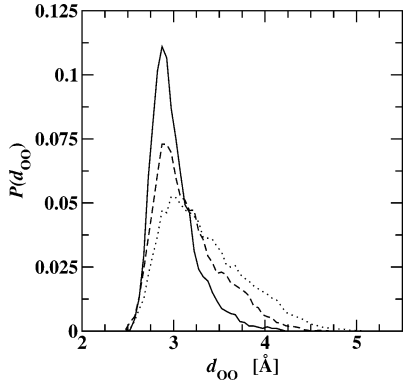

Figure 7. Temperature dependence of the distribution of oxygen−oxygen distances between a given molecule and its four nearest neighbors. The solid, dashed, and dotted lines depict the results at $T =$ 323, 423, and 523 K, respectively.

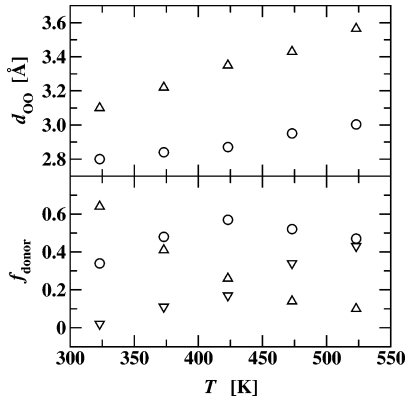

Figure 8. (Top) Temperature dependence of the oxygen−oxygen distances to the two nearest (○) and the two next-nearest (△) molecules in the coordination shell. (Bottom) Temperature dependence of the fraction of double-donor (△), single-donor (○), and nondonor (▽) configurations.

Using the angular-distance criterion suggested by Wernet et al.,[57] a given water molecule can be classified as either being in a double-donor (DD), single-donor (SD), or nondonor (ND) configuration. The temperature dependence of the population of these three species in the saturated liquid phase is depicted in Figure 8. As the temperature increases, the fraction of DD configurations decreases monotonically and that of ND configurations increases monotonically, whereas the fraction of SD shows a weak maximum at intermediate temperatures. At no point does the SD fraction approach 80% as determined by Wernet et al.[57] (see also ref 41). From a plot of the temperature dependence of the equilibrium constant between strong and distorted (or broken) hydrogen bonds in the 4-fold coordination[58] (see Figure 9), we estimate an average thermal enthalpy required for the disappearance of a strong hydrogen bond of 15 kJ/mol, a value that falls within the range from 9 to 16 kJ/mol inferred by Wernet et al.[57] Although on first glance, this value falls above the range of 4−8 kJ/mol obtained by Smith et al.,[58] it should be noted that the saturated liquid density decreases substantially over the temperature range investigated here, while it is nearly constant over the range of the latter experiment. Indeed, if the configurations from the simulations are scaled to a common density, then our computed value is reduced by 40%. Thus, when comparing different data sets on hydrogen bond statistics, it is important to consider the extent of the density change over the temperature interval of interest. A comparison of the enthalpic cost for the loss of strong hydrogen bonds and the change in the heat of vaporization is also instructive. Over the

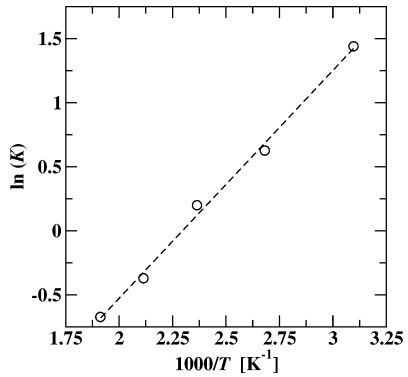

Figure 9. van't Hoff plot of the logarithm of the equilibrium constant between strong and distorted hydrogen bonds in the 4-fold coordination vs the inverse temperature. The dashed line is a linear fit to the simulation data and yields a rearrangement enthalpy of 15 kJ/mol.

200 K range, the number of strong hydrogen bonds decreases from 3.2 to 1.4 for a rearrangement cost of about 27 kJ/mol. The corresponding change in the heat of vaporization is 25 kJ/mol, thus demonstrating that changes in the hydrogen bond population govern the overall energetics.

Another advantage of using a first principles description of the system is that it allows for unbiased changes in molecular conformation and electronic structure. The MC simulations show slight variations in the average bending angle with the value for the vapor phase at 423 K falling about 2° below that for the liquid phase (i.e., the liquid phase's tetrahedral structure causes a widening of the bond angle), thereby indicating the importance of conformational flexibility for first principles water. A similar change in the bond angle from gas-phase monomer and dimer to the liquid phase was previously observed by Silvestrelli and Parrinello.[13]

Electronic Properties. One of the electronic properties that is very sensitive to the environment is the molecular dipole moment. Snapshots of the liquid phase with molecules colored according to their dipole moment and the distribution of dipole moments are depicted in Figures 10 and 11. The molecular dipole moments were computed from maximally localized Wannier functions with the Berry phase scheme.[13,59,60] It can be clearly seen that the average dipole moment in the saturated liquid phase changes substantially along the coexistence line (with averages of 3.0 and 2.5 D at 323 and 523 K, respectively) and that there is a wide distribution at all temperatures (with a full width at half-maximum (fwhm) of about 0.7 D in the liquid phase). Furthermore, as can be seen from Figure 10, there appears to be a spatial correlation in the liquid phase that has molecules of similar dipole moment in close proximity. The variations of the molecular dipole moment in the vapor phase are much smaller (with averages of 1.8 and 2.1 D at 323 and 523 K, respectively).

It is also intructive to compare the molecular dipole moment distribution to experimental and other simulation data. For liquid water at ambient conditions, the best experimental estimate of the average molecular dipole moment is 2.9 ± 0.6 D,[61] and first principles molecular dynamics simulations at $T =$ 318 K and $\rho = 10^3$ kg/m^3 gave a value of 2.9 D with a fwhm of 0.7 D.[13] As can be seen, the molecular dipole moment distribution obtained for the saturated liquid phase at $T =$ 323 K is in good agreement with these data. The dipole moment distributions at the elevated temperatures (see Figure 11) can be compared to those obtained from Car-Parrinello molecular dynamics simulations of supercritical fluid water.[23,24] The average dipole moment of 2.4 D and fwhm of 0.8 observed at $\rho = 730$ kg/m^3 and $T =$

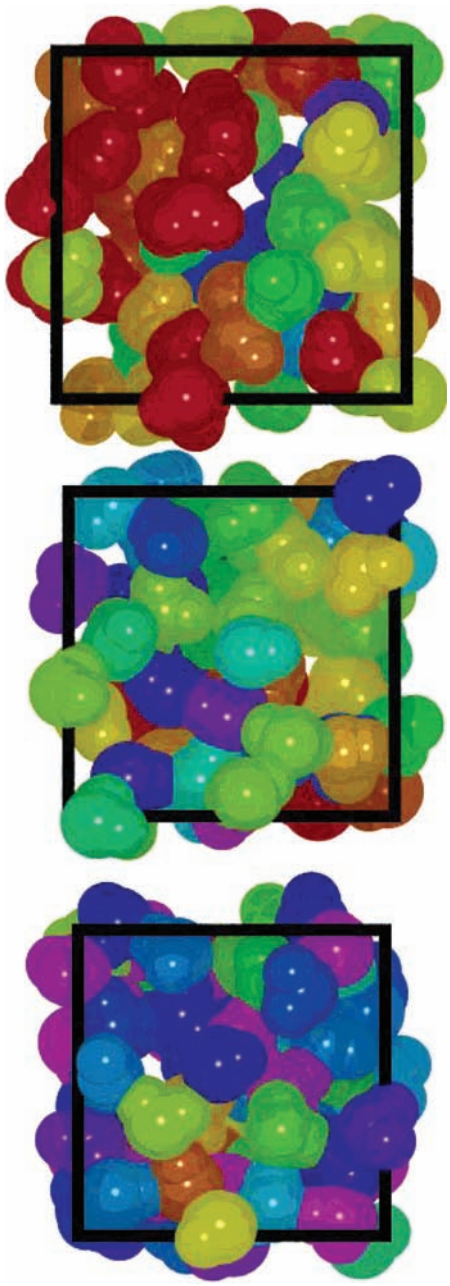

Figure 10. Snapshots of the saturated liquid phase of BLYP-GTH-TZV2P-1200 water at $T = 523$, 423, and 323 K (top to bottom). The molecules are colored according to their instantaneous molecular dipole moment (μ) ranging from red ($\mu < 1.9$ D) to purple ($\mu > 3.2$ D) in intervals of 0.1 D.

653 K[24] is quite similar to the μ distribution found for the saturated liquid phase at $T = 523$ K ($\rho_{sat} \approx 560$ kg/m^3), whereas the μ distribution for the saturated liquid phase at $T = 423$ K ($\rho_{sat} \approx 730$ kg/m^3) is shifted to higher dipole moments as should be expected from a hydrogen-bonding liquid at similar density but much lower temperature. Similarly, the μ distribution obtained for the saturated vapor phase at 523 K qualitatively resembles that found for supercritical fluid water at a higher temperature of 647 K and higher density of 320 kg/m^3.[24]

In addition to the molecular dipole moment, a property that in principle can also be obtained from polarizable water models,[3,43,62−64] the first principles description enables a detailed investigation of other electronic properties. As an example, the spread of the liquid-phase LUMO is shown in Figure 12. The LUMO is very diffuse and spreads over a significant fraction

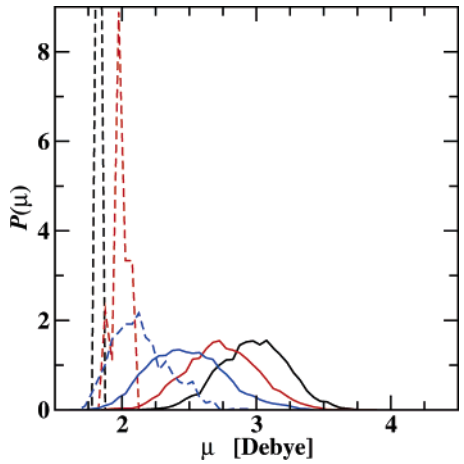

Figure 11. Temperature dependence of the distribution of molecular dipole moments in the saturated liquid (solid lines) and gas (dashed lines) phases. The results at $T = 323$, 423, and 523 K are shown as black, red, and blue lines, respectively.

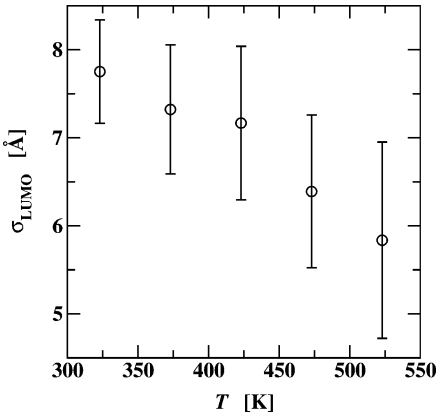

Figure 12. Temperature dependence of the spread of the lowest unoccupied molecular orbital in the liquid. Error bars give the full width half-maximum of the observed ensemble distributions.

of the entire liquid box. This somewhat curious diffuse nature of the LUMO was previously observed for near-ambient liquid water[65] and supercritical fluid water.[24] According to the Anderson model for the localization of electronic states,[66] the decrease in the LUMO spread with increasing temperature is a manifestation of a phase with larger random fluctuations and less contact between neighboring molecules (i.e. less hydrogen bonding).

Conclusions

Advanced Monte Carlo algorithms and an efficient electronic structure program are combined to enable the first calculation of the vapor−liquid coexistence curve for a molecular fluid from first principles. Although the Gibbs ensemble MC simulations of this work are necessarily carried out for a smaller system and shorter run length than is typical for molecular mechanics force fields, the simulations are sufficiently precise to show that the BLYP-GTH-TZV2P-1200 description of water leads to a significant underestimation of the saturated liquid density, the normal boiling point, and the critical temperature. Thus, great care should be exercised when comparing the properties calculated for this water representation (and, maybe, other GGA functionals) with their experimental counterparts at the same absolute state point (e.g., temperature and liquid density).

In future work, the great sensitivity of the phase diagram to the underlying model will allow us to probe nuclear quantum

effects and to evaluate the accuracy of different functionals and the influence of the choice of pseudopotential, basis set, and charge density cutoff. The ability to compute phase equilibria using a first principles description will open the door to investigations of multiphase chemical equilibria and of adsorption isotherms involving proton transfer, bond formation, and/or charge transfer.

Acknowledgment. We thank Michele Parrinello, Michiel Sprik, Larry Fried, and Charlie Westbrook for their ongoing support of this work and David Chandler for a critical reading of this manuscript. Financial support from the National Science Foundation through grants CTS-0138393 and ITR-0428774 (VLab), the Engineering and Physical Sciences Research Council, a Department of Energy Computational Science Graduate Fellowship (M.J.M.), and a 3M Foundation Fellowship (M.J.M.) is gratefully acknowledged. Part of this work was performed under the auspices of the U.S. Department of Energy by the University of California Lawrence Livermore National Laboratory (LLNL). J.I.S. and M.J.M. thank the University Relations Program (LLNL) for hosting their sabbatical visit.

References and Notes

(1) Stillinger, F. H. *Science* **2004**, *209*, 451.

(2) Hansen, J. P.; McDonald, I. R. *Theory of Simple Liquids*, 2nd ed.; Academic Press: New York, 1986.

(3) Guillot, B. *J. Mol. Liq.* **2002**, *101*, 219.

(4) Barker, J. P.; Watts, R. O. *Chem. Phys. Lett.* **1969**, *3*, 144.

(5) de Pablo, J. J.; Prausnitz, J. M.; Strauch, H. J.; Cummings, P. T. *J. Chem. Phys.* **1990**, *93*, 7355.

(6) Sans, E.; Vega, C.; Abascal, J. L. F.; MacDowell, L. G. *Phys. Rev. Lett.* **2004** *92*, 5701.

(7) Keutsch, F. N.; Saykally, R. *Proc. Natl. Acad. Sci. U.S.A.* **2001**, *98*, 10533.

(8) Chen, B.; Siepmann, J. I.; Klein, M. L. *J. Chem. Phys. A* **2005**, *109*, 1137.

(9) Cavazzoni, C.; Chiarotti, G. L.; Scandolo, S.; Tosatti, E.; Bernasconi, M.; Parrinello, M. *Science* **1999**, *283*, 44.

(10) Goncharov, A. F.; Goldman, N.; Fried, L. E.; Crowhurst, J. C.; Kuo, I-F. W.; Mundy, C. J.; Zaug, J. M. *Phys. Rev. Lett.* **2005**, *94*, 5508.

(11) Car, R.; Parrinello, M. *Phys. Rev. Lett.* **1985**, *55*, 2471.

(12) Laasonen, K.; Sprik, M.; Parrinello, M.; Car, R. *J. Chem. Phys.* **1993**, *99*, 9080.

(13) Silvestrelli, P. L.; Parrinello, M. *J. Chem. Phys.* **1999**, *111*, 3572.

(14) Hura, G.; Russo, R.; Glaeser, R. M.; Head-Gordon, T.; Krack, M.; Parrinello, M. *Phys. Chem. Chem. Phys.* **2003**, *5*, 1981.

(15) Grossman, J. C.; Schwegler, E.; Draeger, E. W.; Gygi, F.; Galli, G. *J. Chem. Phys.* **2004**, *120*, 300.

(16) Schwegler, E.; Grossman, J. C.; Gygi, F.; Galli, G. *J. Chem. Phys.* **2004** *121*, 5400.

(17) Sit, P. H.-L.; Marzari, N. *J. Chem. Phys.* **2005**, *122*, 204510.

(18) Fernandez-Serra, M. V.; Artacho, E. *J. Chem. Phys.* **2004**, *121*, 11136.

(19) Kuo, I-F. W.; Mundy, C. J.; McGrath, M. J.; Siepmann, J. I.; VandeVondele, J.; Sprik, M.; Hutter, J.; Chen, B.; Klein, M. L.; Mohamed, F.; Krack, M.; Parrinello, M. *J. Phys. Chem. B* **2004**, *108*, 12990.

(20) Kuo, I-F. W.; Mundy, C. J.; McGrath, M. J.; Siepmann, J. I.; *J. Phys. Chem. B*, in preparation.

(21) The first principles simulations studies reported in refs 15−19 have pointed to a room temperature liquid phase for popular generalized gradient approximation functionals that is over-structured and shows too low diffusion coefficients as compared to the experiment. However, these simulations were all carried out at the experimental equilibrium density. Unfortunately, ambient conditions are defined by temperature and pressure (not density), and these simulations are therefore unsuited for a stringent assessment of the accuracy of DFT water representations at ambient conditions. Indeed, two recent simulation studies[27, 35] point to a significant underestimation of the ambient equilibrium density for the BLYP functional, and this substantial decrease in density results in significant structural changes as compared to simulations done at the experimental density (i.e., elevated pressure for the DFT model).

(22) Fois, E. S.; Sprik, M.; Parrinello, M. *Chem. Phys. Lett.* **1994**, *223*, 411.

(23) Boero, M.; Terakura, K.; Ikeshoji, T.; Liew, C. C.; Parrinello, M. *Phys. Rev. Lett.* **2000**, *85*, 3245.

(24) Boero, M.; Terakura, K.; Ikeshoji, T.; Liew, C. C.; Parrinello, M. *J. Chem. Phys.* **2001**, *115*, 2219.

(25) Geissler, P. L.; Dellago, C.; Chandler, D.; Hutter, J.; Parrinello, M. *Science* **2001**, *291*, 2121.

(26) Tuckerman, M. E.; Marx, D.; Parrinello, M. *Nature* **2002**, *417*, 925.

(27) Kuo, I-F. W.; Mundy, C. J. *Science* **2004**, *303*, 658.

(28) Asthagiri, D.; Pratt, L. R.; Kress, J. D. *Phys. Rev. E* **2003**, *68*, 041505.

(29) Thomson, K. T.; Wentzcovitch, R. M.; Bukowinski, M. S. T. *Science* **1996**, *274*, 1880.

(30) Vocadlo, L.; Alfe, D.; Gillan, M. J.; Wood, I. G.; Brodholt, J. P.; Price G. D. *Nature* **2003**, *424*, 536.

(31) Panagiotopoulos, A. Z. *Mol. Phys.* **1987**, *61*, 813.

(32) Lippert, G.; Hutter, J.; Parrinello, M. *Mol. Phys.* **1997**, *92*, 477.

(33) VandeVondele, J.; Krack, M.; Mohamed, F.; Parrinello, M.; Chassaing, T.; Hutter, J. *Comput. Phys. Comm.* **2005**, *167* 103.

(34) McDonald, I. R. *Mol. Phys.* **1972**, *23*, 41.

(35) McGrath, M. J.; Siepmann, J. I.; Kuo, I-F. W.; Mundy, C. J.; VandeVondele, J.; Hutter, J.; Mohamed, F.; Krack, M. *ChemPhysChem* **2005**, *6*, 1849.

(36) Siepmann, J. I.; Frenkel, D. *Mol. Phys.* **1992**, *75*, 59.

(37) Smit, B.; Karaborni, S.; Siepmann, J. I. *J. Chem. Phys.* **1995**, *102*, 2126.

(38) McGrath, M. J.; Siepmann, J. I.; Kuo, I-F. W.; Mundy, C. J.; VandeVondele, J.; Sprik, M.; Hutter, J.; Mohamed, F.; Krack, M.; Parrinello, M. *Comput. Phys. Comm.* **2005**, *169*, 289.

(39) Izvekov, S.; Parrinello, M.; Burnham, C. J.; Voth, G. A. *J. Chem. Phys.* **2004**, *120*, 10896.

(40) Vlugt, T. J. H.; Martin, M. G.; Smit, B.; Siepmann, J. I.; Krishna, R. *Mol. Phys.* **1998**, *94*, 727.

(41) Silvestrelli, P. L.; Bernasconi, M.; Parrinello, M. *Chem. Phys. Lett.* **1997**, *277*, 478.

(42) Gregory, J. K.; Clary, D. C.; Liu, K.; Brown, M. G.; Saykally, R. J. *Science* **1997**, *275*, 814.

(43) Chen, B.; Potoff, J. J.; Siepmann, J. I. *J. Phys. Chem. B* **2000**, *104*, 2378.

(44) Jorgensen, W. L.; Chandrasekhar, J.; Madura, J. D.; Impey, R. W.; Klein, M. L. *J. Chem. Phys.* **1983**, *79*, 926.

(45) Becke, A. D. *Phys. Rev. A* **1988**, *38*, 3098.

(46) Lee, C.; Yang, W.; Parr, R. C. *Phys. Rev. B* **1988**, *37*, 785.

(47) Goedecker, S.; Teter, M.; Hutter, J. *Phys. Rev. B* **1996**, *54*, 1703.

(48) Hartwigsen, C.; Goedecker, S.; Hutter, J. *Phys. Rev. B* **1998**, *58*, 3641.

(49) Boese, A. D.; Martin, J. M. L.; Handy, N. C. *J. Chem. Phys.* **2003**, *119*, 3005.

(50) Shinoda, W.; Shiga, M. *Phys. Rev. E* **2005**, *71*, 041204.

(51) Mantz, Y. A.; Chen, B.; Martyna, G. J. *Chem. Phys. Lett.* **2005**, *405*, 294.

(52) Balog, E.; Hughes, A. L.; Martyna, G. J. *J. Chem. Phys.* **2000**, *112*, 870.

(53) The saturated vapor pressures were estimated from the directly computed saturated vapor density applying the virial expression (truncated at the second virial coefficent that was calculated for the pre-sampling potential[39]).

(54) NIST Chemistry Webbook (http://webbook.nist.gov).

(55) VandeVondele, J.; Mohamed, F.; Krack, M.; Hutter, J.; Sprik, M.; Parrinello, M. *J. Chem. Phys.* **2005**, *122*, 014515.

(56) Dahlke, E. E.; Truhlar, D. G. *J. Phys. Chem. B* **2005**, *109*, 15677.

(57) Wernet, Ph.; Nordlund, D.; Bergmann, U.; Cavalleri, M.; Odelius, M.; Ogasawara, H.; Näslund, L. Å.; Hirsch, T. K.; Ojamäe, L.; Glatzel, P.; Petterson, L. G. M.; Nilsson, A. *Science* **2004**, *304*, 995.

(58) Smith, J. D., Cappa, C. D.; Wilson, K. R.; Messer, B. M.; Cohen, R. C.; Saykally, R. J. *Science* **2004**, *306*, 851.

(59) Marzari, N.; Vanderbilt, D. *Phys. Rev. B* **1997**, *56*, 12847.

(60) King-Smith, R. D.; Vanderbilt, D. *Phys. Rev. B* **1993**, *47*, 1651.

(61) Badyal, Y. S.; Saboungi, M.-L.; Price, D. L.; Shastri, S. D.; Haeffner, D. R.; Soper, A. K. *J. Chem. Phys.* **2000**, *112*, 9206.

(62) Dang, L. X. *J. Phys. Chem. B* **1998**, *102*, 620.

(63) Chen, B.; Xing, J.; Siepmann, J. I. *J. Phys. Chem. B* **2000**, *104*, 2391.

(64) Paricaud, P.; Predota, M.; Chialvo, A. A.; Cummings, P. T. *J. Chem. Phys.* **2005**, *122*, 244511.

(65) Laasonen, K.; Sprik, M.; Parrinello, M. In *Ultrafast Reaction Dynamics and Solvent Effects*; Gauduel, Y., Rossky, P. J., Eds.; AIP Conference Proceedings Vol. 298; AIP: New York, 1994; p 87.

(66) Anderson, P. W. *Phys. Rev.* **1958**, *109*, 1492.